CHAPTER VI
RESULTS AND DISCUSSION

4.1 Standard Chemicals Analysis

The reference standards for gas products were analyzed by an Agilent HP-5890 equipped with flame ionized detector (FID) with a capillary HP-PLOT/Al_2O_3. It was found that the retention times for methane, ethane, ethylene, propane, propylene, butane acetylene, 1-butene and i-butene were 0.768, 0.995, 1.147, 1.522, 3.907, 4.501, 4.927, 7.721 and 8.151 min, respectively, as shown in Figure 4.1.

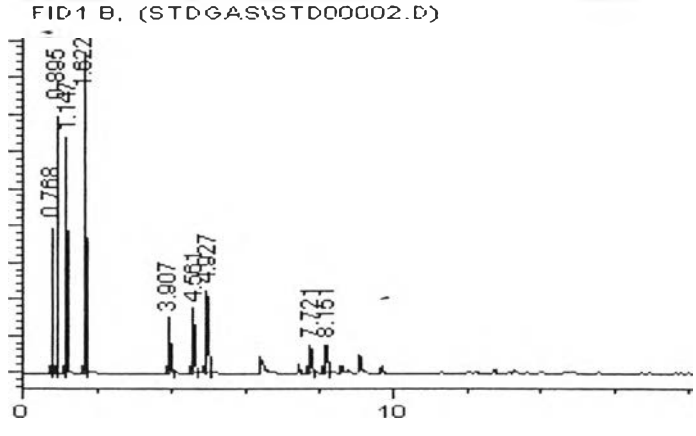

Figure 4.1 Chromatogram of standard gas mixture.

Standard chemicals for liquid products were analyzed by an Agilent HP-6890 gas chromatograph equipped with flame ionized detector (FID) with HP-INNOWAX column. Since liquid product was obtained with 2 phases—hydrocarbons and oxygenates. The analysis was done separately. Standard hydrocarbons exhibited the retention time of C_5, C_6, C_7, benzene, toluene, *p*-xylene, *m*-xylene and *o*-xylene were 4.957, 5.120, 5.430, 7.659, 9.310, 11.566, 11.771 and 13.211 respectively, as shown in Figure 4.2.

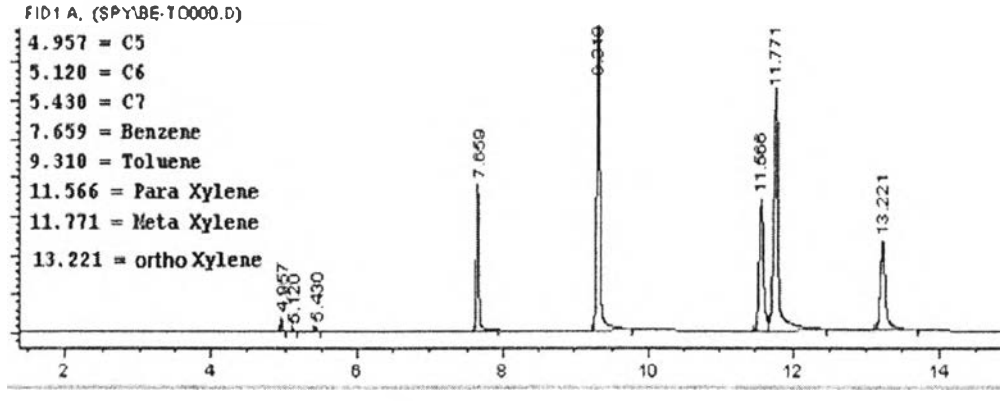

Figure 4.2 Chromatogram of standard liquid mixture in hydrocarbon phase.

A mixture of oxygenate standards contained acetaldehyde, propanal, acetone, methanol, ethanol, *n*-propanol, *n*-butanol, and acetic acid. It was found that the retention times of acetaldehyde, propanal, acetone, methanol, ethanol, *n*-propanol, *n*-butanol, and acetic acid were 5.329, 5.858, 6.067, 6.752, 7.174, 8.868, 11.00 and 23.764 min, respectively as shown in Figure 4.3.

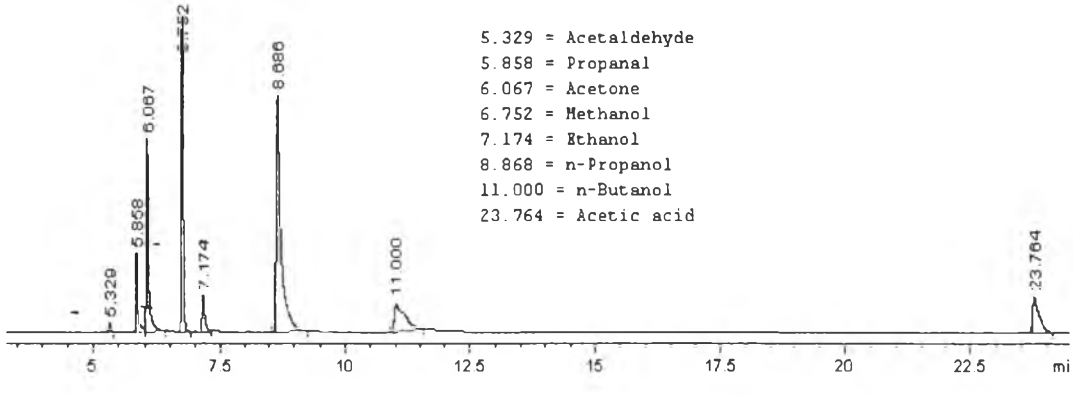

Figure 4.3 Chromatogram of standard liquid mixture oxygenate phase.

To find out the response factor of each compound, *n*-hexane was used as the reference. Table 4.1 shows the response factor of each substance in the reference standard which contains (1-propanol, propen-2-ol, methanol, ethanol, *n*-propanol, *n*-butanol, acetone, acetol, acetic acid, and acetaldehyde). For low boiling point compounds, it is difficult to obtain the response factor because it is volatile chemical.

Table 4.1 Response factors of the potential intermediately and products

Substances	Formula	Response factor
1-Propanol	C_3H_8O	0.651
n-Propanol	C_3H_8O	0.651
Propen-2-ol	C_3H_6O	0.468
Methanol	CH_4O	0.355
Ethanol	C_2H_6O	0.521
Acetone	C_3H_6O	0.491
Acetaldehyde	C_2H_4O	0.502
Acetol	$C_3H_6O_2$	0.293
Acetic acid	$C_2H_4O_2$	0.217
n-Butanol	$C_4H_{10}O$	0.721

4.2 Catalyst Characterization

4.2.1 Brunauer-Emmett-Teller Method (BET)

BET technique was used to investigate the surface area and pore volume of the parent HZSM-5 and alkali treated HZSM-5. The results are summarized in Table 4.2. The surface area of the alkali treated HZSM-5 decreased in the following order: 0.3ATHZ > 0.1 ATHZ > HZSM-5(30) > 0.5 ATHZ > 1 ATHZ. For 0.1 ATHZ and 0.3 ATHZ, they resulted in increasing surface area, external surface area and micro pore volume. When the concentration of NaOH was higher than 0.3 M, surface area and micropore volume were deceased. The results indicated that the micropore structure has been destroyed due to the severe desilication. For catalyst 1 ATHZ, the external surface area was 272.3 m^2/g, and the micropore surface area was zero because the microporous structure of zeolite was collapsed due to the rupture of Si–O bonds during the NaOH treatment. Moreover, the severe desilication led to the destruction of the zeolite framework, which was disadvantageous not only for the micropores but also for the formation of mesopores (Zhao *et al.*, 2010).

Table 4.2 Textural properties of the parent HZSM-5 and alkali treated HZSM-5

Catalysts	Surface area (m^2/g)	Micropore surface area[a] (m^2/g)	External surface area[a] (m^2/g)	Total pore volume[b] (mL/g)	Micropore volume[a] (mL/g)
HZSM-5(30)	382.4	265.7	116.7	0.521	0.129
0.1ATHZ	394.7	260.2	134.5	0.576	0.126
0.3 ATHZ	398.1	250.2	147.9	0.585	0.122
0.5 ATHZ	367.8	199.6	168.2	0.627	0.100
1 ATHZ	272.3	0	272.3	0.644	-

Using [a] T-plot, [b] Volume adsorbed at $P/P_0 = 0.99$

Table 4.3 Textural properties of the parent HZSM-5 and silylated HZSM-5 catalysts

Catalysts	Surface area[a] (m^2/g)	Micropore surface area[b] (m^2/g)	External surface area[b] (m^2/g)	Total pore volume (mL/g)	Micropore volume[a] (mL/g)
HZSM-5(30)	382.4	265.7	116.7	0.521	0.129
20CLD	327.9	262.8	65.1	0.398	0.129
0.3AT20CLD	353.4	272.1	81.3	0.453	0.134
2Cy20CLD	288.9	220.0	68.9	0.412	0.108

Using [a] T-plot, [b] Volume adsorbed at $P/P_0 = 0.99$

Deposition of an inert silica layer on the external surface of HZSM-5 resulted in the decrease in surface area, total pore volume, and micropore volume. The results indicated that the silylation could block some of the HZSM-5 micropores. Therefore, the surface area and pore volume of silylated HZSM-5 (20CLD, 0.3AT20CLD and 2Cy20CLD) were less than those of the parent HZSM-5(30) zeolite. Moreover, it was clearly seen that surface area and pore volume were decreased as the degree of silylation increased.

4.2.2 X-ray Fluorescence Spectroscopy

XRF results showed that the Si/Al ratio of the parent HZSM-5 and alkali treated HZSM-5 were dramatically decreased from 31.6 to 20.4 (0.5 ATHZ) with NaOH concentration increasing from 0 to 1.0 M as shown in Table 4.4, indicating that the Si was preferentially extracted than Al in the zeolite. This is interpreted that the Si-O-Si bond is relatively easier for cleavage compared to the Si-O-Al bond in the presence of OH^- because of the negative charge AlO^{4-} tetrahedron. Such a desilication process is clearly dependent on the concentration of NaOH solution, and higher *p*H values favor the preferential extraction of Si, resulting in the relatively high Al content in the zeolite (Li *et al.*, 2008).

The silylated HZSM-5 samples were analyzed by XRF. Table 4.4 shows the amount of SiO_2 and Si/Al molar ratio increased with increasing deposition inert silica TEOS loading.

Table 4.4 Si/Al ratios and $\%NaO_2$ of parent HZSM-5, alkali treated HZSM-5, and silylated HZSM-5

Catalysts	$\%SiO_2$	$\%Al_2O_3$	$\%NaO_2$	Si/Al
HZSM-5	94.90	5.11	-	31.6
0.1 ATHZ	94.08	5.92	0.12	27.0
0.3 ATHZ	93.30	6.70	0.29	23.7
0.5 ATHZ	92.32	7.68	0.48	20.4
0.75 ATHZ	n.a.	n.a.	0.59	n.a.
1 ATHZ	n.a.	n.a.	1.72	n.a.
20CLD	95.91	4.10	n.a.	39.8
0.3AT20CLD	95.15	4.59	0.26	35.2
2Cy20CLD	96.64	3.36	n.a.	48.9

4.2.3 Temperature Programmed Desorption (TPD) of Isopropylamine

The Brønsted acid sites of parent HZSM-5 and alkali treated HZSM-5 analyzed by TPD of isopropylamine are summarized in Table 4.5. Comparing among parent HZSM-5 and alkali treated HZSM-5, the Brønsted acid sites of the catalysts decreased in the following order: HZSM-5(30) > 0.1 ATHZ > 0.3 ATHZ > 0.5 ATHZ > 0.75 ATHZ > 1 ATHZ. The alkali treatment with high NaOH concentration not only resulted in the remove Si atom, but also removed some of Al atoms from the zeolite framework, which caused the destruction of zeolite structure and the loss of strong acid sites (Ni *et al.*, 2011), leading to the decease of the density of acid sites and Brønsted acidity of treated HZSM-5. This was probably because Na^+ replace H^+ on HZSM-5. Whereas the Brønsted acidity significantly decreases when the NaOH concentration increased from 0.5 to 1 M. This might be result from the collapse of zeolite framework. The proper alkali treatment could slightly decrease Brønsted acid site.

Table 4.5 Brønsted acid sites of the parent HZSM-5 ,alkali treated HZSM-5 and silylated HZSM-5 from TPD of isopropylamine

Catalysts	Brønsted Acid (μmol/g)
HZSM-5	414
0.1ATHZ	387
0.3ATHZ	378
0.5ATHZ	288
0.75ATHZ	226
1 ATHZ	215
20CLD	356
0.3AT20CLD	320
2Cy20CLD	226

Figure 4.4 shows the TPD profiles of isopropylamine of the parent HZSM-5 and alkali treated HZSM-5 (30) with different NaOH concentrations. The quantification of the Brønsted acid sites was done by monitoring the desorption of propylene. It was clearly seen that the peak centered at 380 °C represented Brønsted

acid sites because propylene produced on the Brønsted acid sites and desorbed at this temperature (Gorte *et. al.*, 1992). From the observation, the peak position of Brønsted acid sites was slightly shifted to lower temperature with increasing concentration of alkali solution (Zheng. *et al*, 2008). It was suggested that the destruction of zeolite structure could cause the loss of strong acid sites (Li *et al.*, 2008).

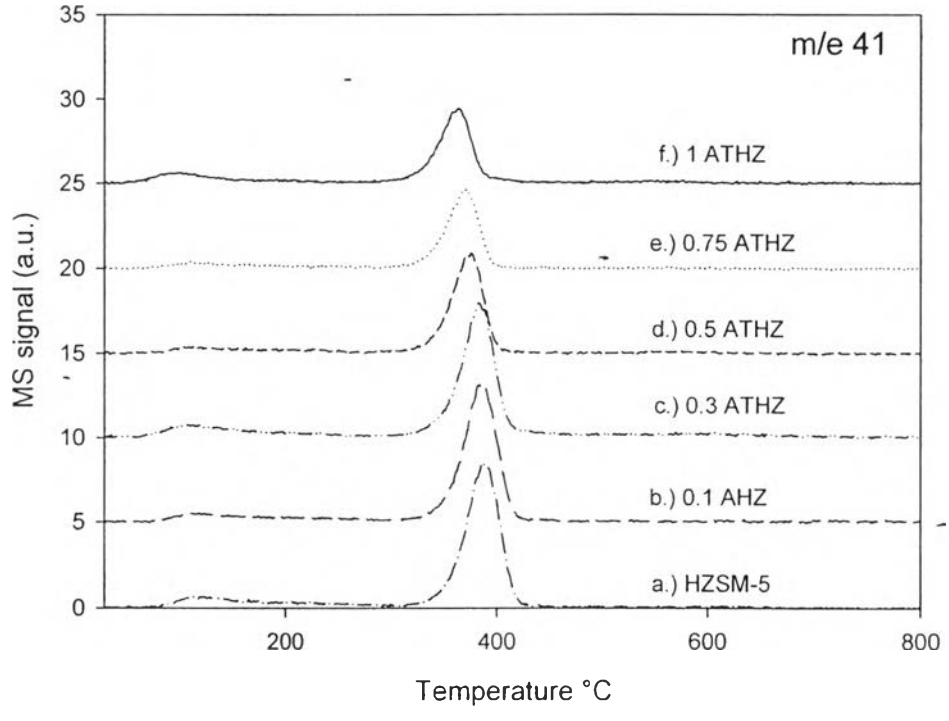

Figure 4.4 Isopropylamine-TPD profiles of the HZSM-5, 0.1 ATHZ, 0.3 ATHZ, 0.5 ATHZ, 0.75 ATHZ and 1 ATHZ, the peaks monitored was propylene (*m/e*=41).

Figure 4.5 shows the TPD profiles of HZSM-5(30), 20CLD, 0.3AT20CLD and 2Cy20CLD. As mentioned earlier, amount of Brønsted acid site was remarkably decreased because the external acid sites were deactivated by the deposited inert silica layer via CLD technique. All catalysts showed that, no difference in the peak position which could be implied that silylation process did not change the acid strength of the catalysts.

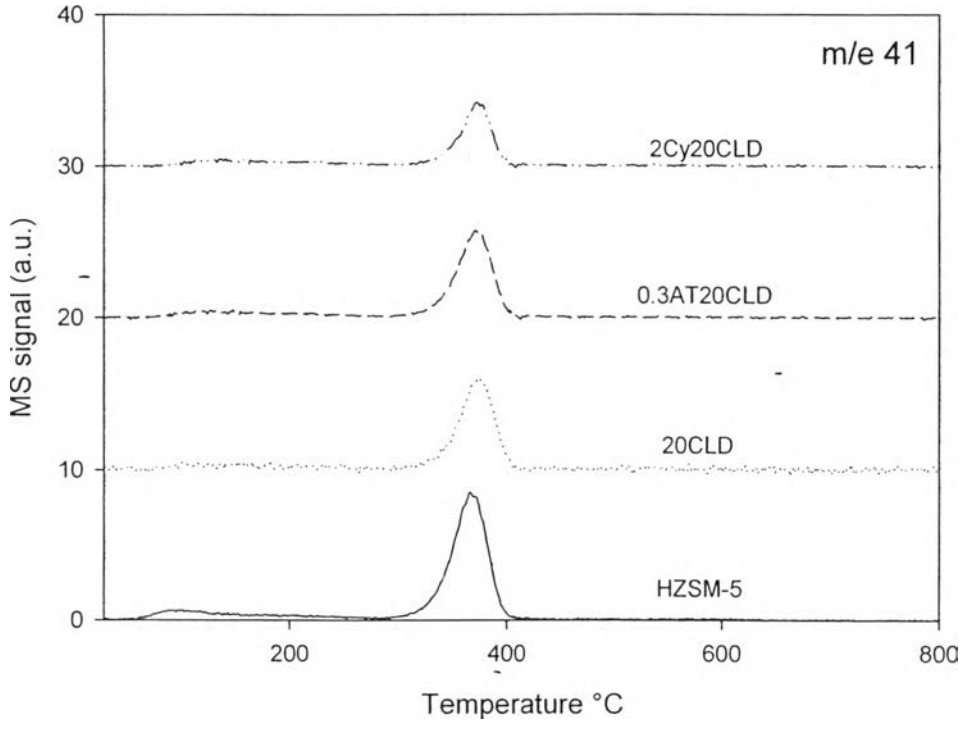

Figure 4.5 Isopropylamine-TPD profiles of the HZSM-5, 20CLD, 0.3 ATHZ20CLD, and 2Cy20CLD peaks monitored was propylene (*m/e*=41).

4.2.4 Temperature Programmed Desorption (TPD) of Ammonia

NH_3-TPD profiles are reported in Figure 4.6. The NH_3-TPD profile of HZSM-5 zeolites consisted of two desorption peaks, low-temperature peak and high-temperature peak. Generally, the high-temperature peak can be ascribed to the absorption of ammonia on strong acid sites, whereas the low-temperature peak was assigned to weak adsorption sites of ammonia. The acidity and acid strength of the zeolites were obviously decreased with the following order of HZSM-5 > 0.1ATHZ > 0.3ATHZ > 1 ATHZ > 20CLD and 2Cy20CLD. The alkali treated HZSM-5 was described the destruction of zeolite structure that causing the loss of strong acid sites (Li *et al.*, 2008). In addition, Na+ from alkali treatment could replace H^+ on HZSM-5. For silylated HZSM-5 the external acid sites were deactivated by the deposited inert silica layer via CLD technique, so the NH_3-TPD from alkali treated HZSM-5 and silylated HZSM-5 less adsorbed than parent HZSM-5.

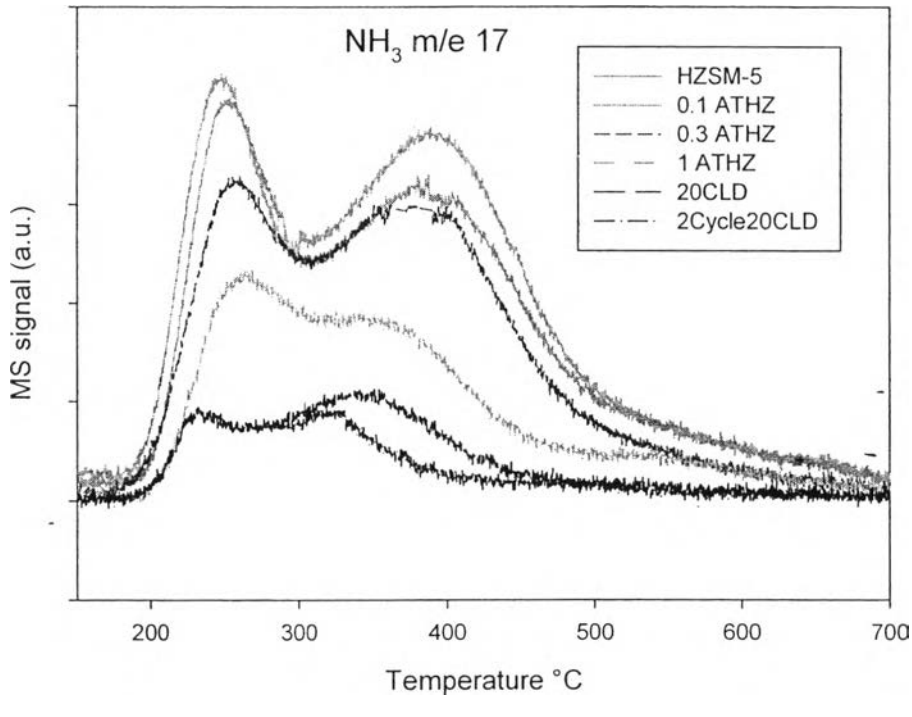

Figure 4.6 Ammonia-TPD profiles of the HZSM-5, 0.1 ATHZ, 0.3 ATHZ, 1 ATHZ, 20CLD and 2Cy20CLD the peaks monitored was propylene (*m/e*=17).

4.2.5 X-ray Diffraction (XRD)

To confirm the zeolite structure and crystallinity of the catalyst, XRD was conducted on the alkali treated HZSM-5 catalysts as shown in Figure 4.7. It was clearly seen that the alkali treatment process did not change the crystallinity of the parent HZSM-5 catalyst. The crystallinity of HZSM-5 zeolite was mainly preserved at the NaOH concentration of 0.3 M. For 1.0 ATHZ, the characteristic diffraction peaks corresponding to HZSM-5 zeolite still remained, but the degree of crystallinity was decreased (Li *et al.*, 2008).

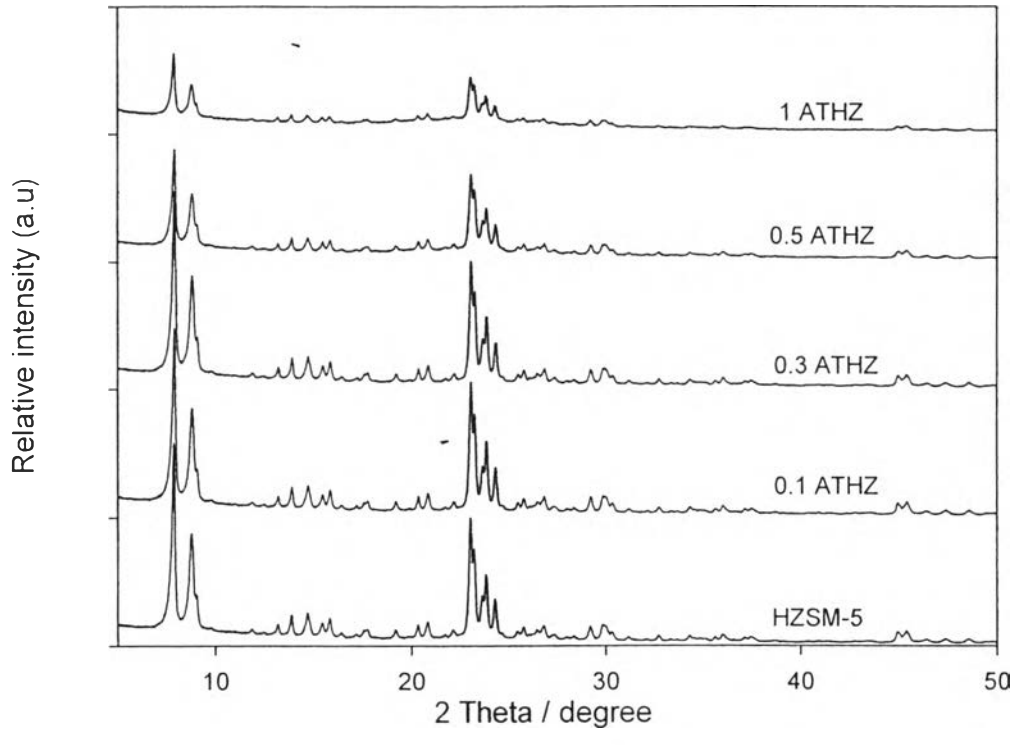

Figure 4.7 XRD patterns of HZSM-5, 0.1 ATHZ, 0.3 ATHZ, 0.5 ATHZ and 1 ATHZ.

Figure 4.8 shows the XRD patterns of silylated HZSM-5. The results showed the silylated zeolites contained HZSM-5 crystalline phase. This indicates that the silylation process did not affect the HZSM-5 framework structure.

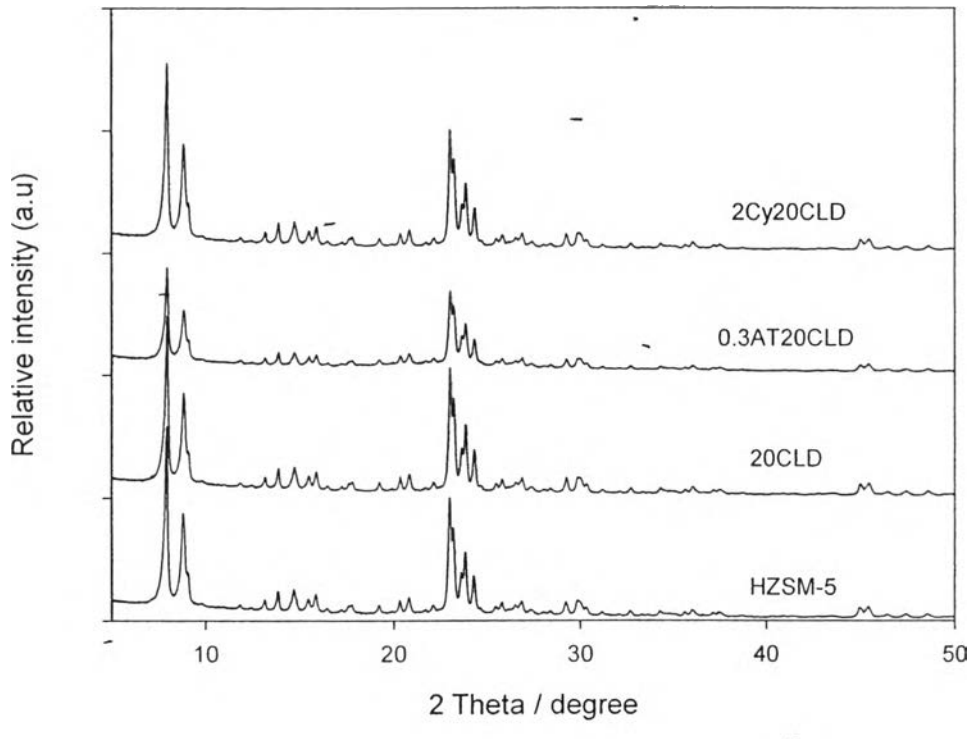

Figure 4.8 XRD patterns of HZSM-5, 20CLD, 0.3AT20CLD and 2Cy20CLD.

4.2.6 Scanning Electron Microscope (SEM)

The morphologies of the different zeolite samples are shown in Figures 4.9 and 4.10. The alkali treated HZSM-5 slightly changed in the morphology of parent HZSM-5. Because the alkali treatment could create several pores and holes, appearing on the zeolite surface (Zhao *et al.*, 2011). The particle sizes of the parent were deceased after treatment in 0.5 M NaOH solution. This result indicated the occurrence of crystal deagglomeration (Li *et al.*, 2008). Further increasing the NaOH concentration to 1.0 M resulted in more non-uniform particles. The edges of the particles melted became to very irregular, indicating that the severe desilication had destroyed some part of the zeolite framework under the experimental condition.

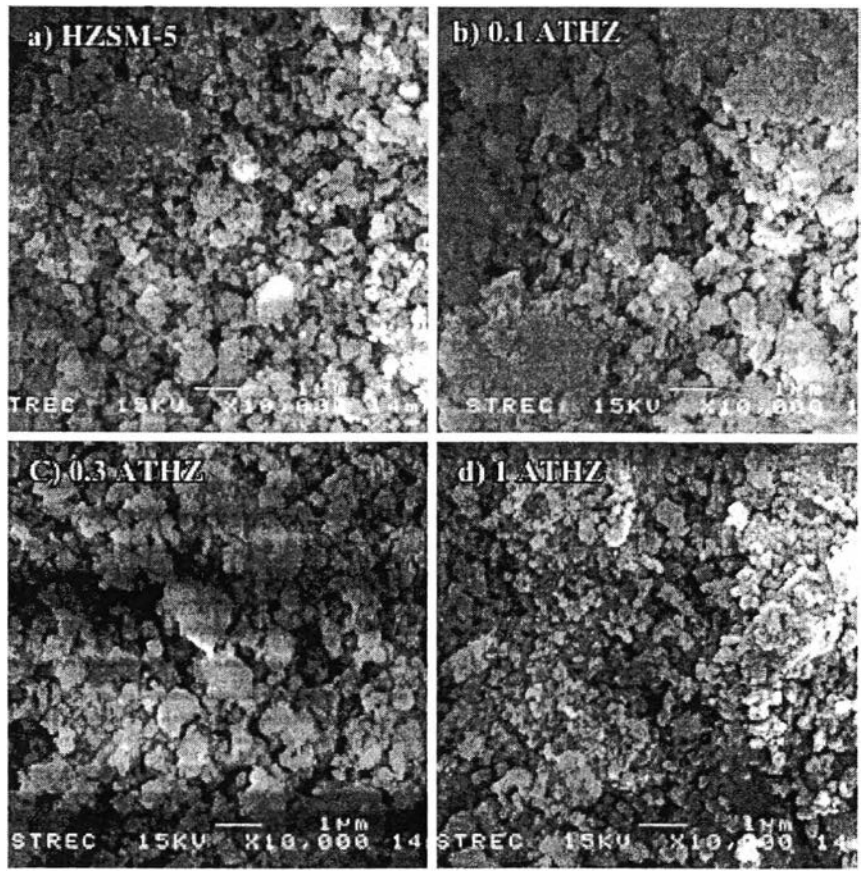

Figure 4.9 SEM images of HZSM-5 zeolites a) parent HZSM-5, b) alkali treated HZSM-5 with 0.1 M NaOH, c) alkali treated HZSM-5 with 0.3 M NaOH, d) alkali treated HZSM-5 with 1 M NaOH.

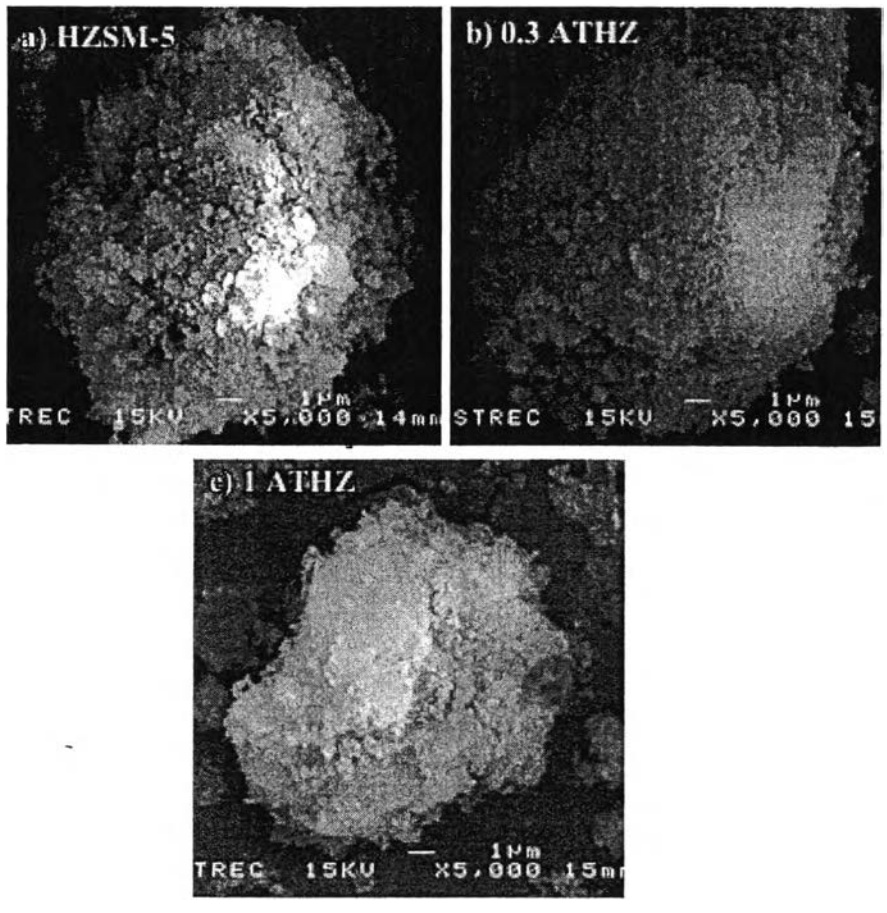

Figure 4.10 SEM images of HZSM-5 zeolites a) parent HZSM-5, b) alkali treated HZSM-5 with 0.3 M NaOH, c) alkali treated HZSM-5 with 1 M NaOH.

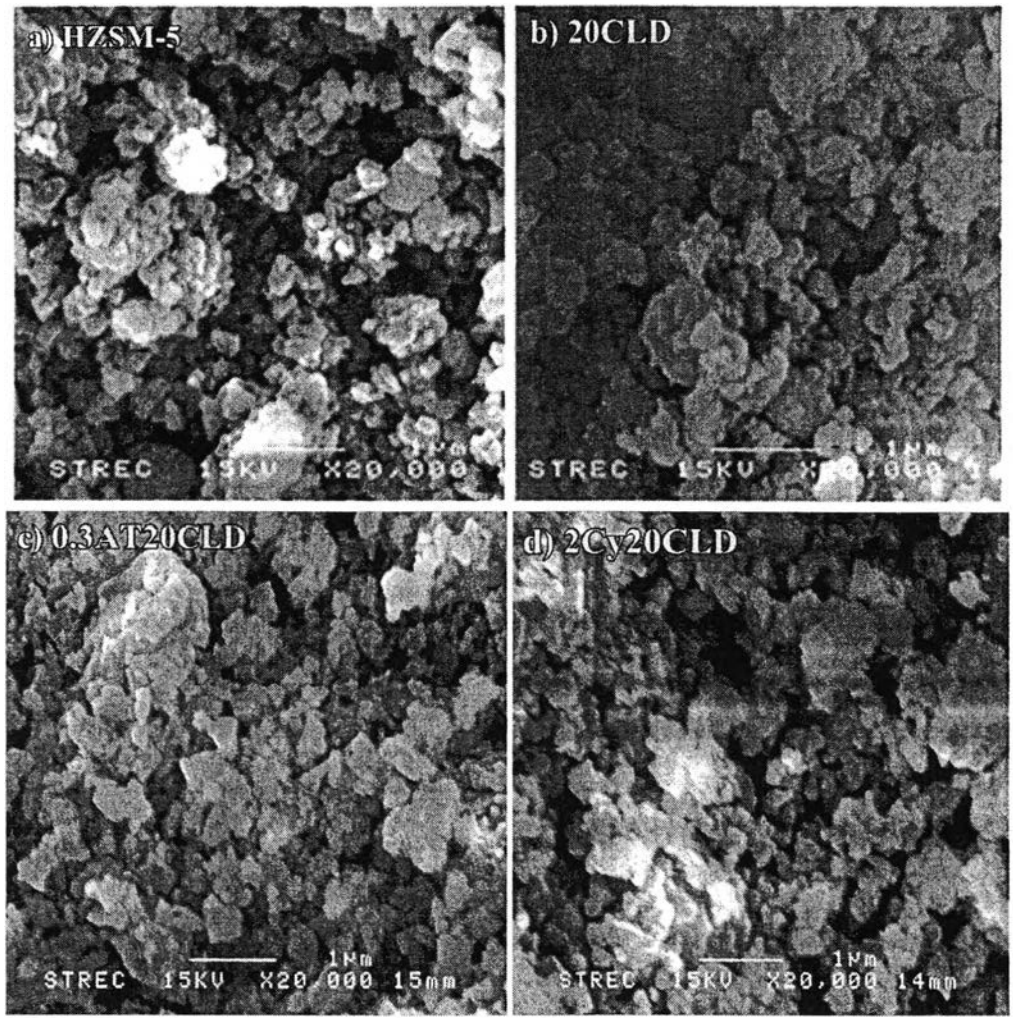

Figure 4.11 SEM images of HZSM-5 zeolites a) HZSM-5, b) 20CLD, c) 0.3AT20CLD, and d) 2Cy20CLD.

Figure 4.11 shows the SEM images for the alkali treated HZSM-5 and silylated HZSM-5. It could be seen that the external surface of HZSM-5 zeolite crystal was covered by a dense layer of amorphous silica, resulting from the TEOS-CLD treatment. It could deactivate the acid sites on the external surface and further regulate the pore mouth of HZSM-5 zeolite (Teng *et al.*, 2011).

4.3 Catalytic Activity Testing

The catalytic activity of biomass-derived alcohols was carried in a fixed bed stainless steel reactor at 450 °C under atmospheric pressure. The parent HZSM-5, alkali treated and silylate HZSM-5 were pressed into pellets, ground and sieved into the size of 20−40 mesh for catalytic tests. The weight hourly space velocity (WHSV) was varied in the range of 1-50 h^{-1}. All zeolites were pretreated in a nitrogen flow at 450 °C for 1 h. The liquid products were collected in an ice-cooled trap and separated into two phases (hydrocarbon and oxygenate) and gaseous were analyzed with GC-FID.

4.3.1 Effect of Biomass-derived Alcohol Feedstocks

The biomass-derived alcohols including methanol, ethanol, *n*-propanol and *n*-butanol readily reacted on the acid catalysts and all the feeds were completely converted 100% on parent HZSM-5 and treated HZSM-5 under testing conditions.

Figure 4.12 shows the selectivity of aromatic, benzene, toluene, xylenes, C_9+aromatics and *p*-xylene in xylenes over parent HZSM-5 with different biomass-derived alcohols at the third hour of time on stream.

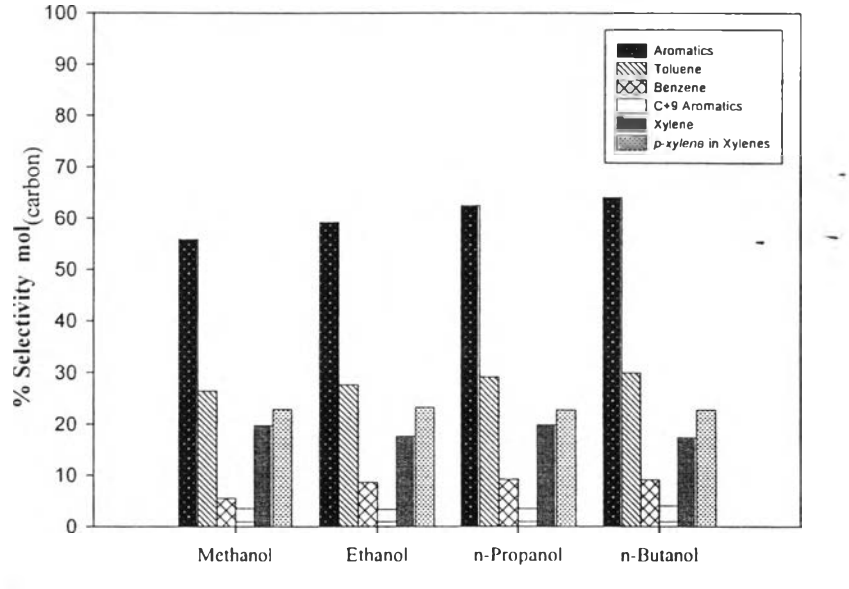

Figure 4.12 Effect of biomass-derived alcohols on aromatic products selectivity and *p*-xylene selectivity in xylenes (Reaction conditions: 450 °C, 14.7 psig, W/F= 0.3 h, and TOS = 3 h).

The aromatics selectivity was decreased in the following order: *n*-butanol > *n*-propanol > ethanol > methanol. The results agreed well with the theoretical yields of aromatics based on the number of carbon atoms. The longer chain alcohols can produced more aromatics hydrocarbons than the shorter chain alcohols (Gujar *et al.*, 2009). To expand the feedstock of this reaction, the aromatization of biomass-derived feedstocks were also carried out HZSM-5 catalyst (Table 4.6). The selectivity to BTX exceeds 50% and product distributions are very similar, in which light hydrocarbons, toluene and xylene are main products.

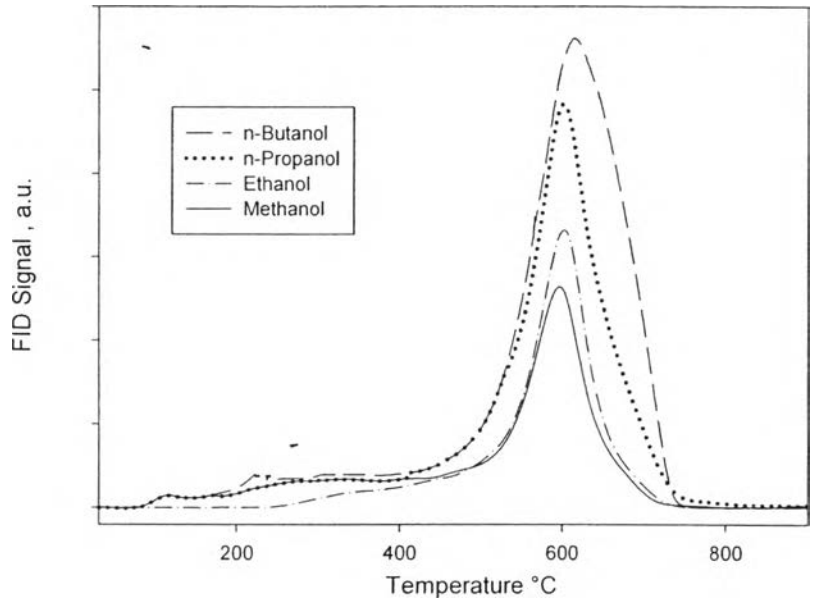

Figure 4.13 TPO profiles of spent HZSM-5 from each feedstock (Reaction conditions: 450 °C, 14.7 psig, W/F= 0.3 h, and TOS = 3 h)

Table 4.6 The product yields and conversion of biomass-derived alcohols over the HZSM-5. (Reaction conditions: 450 °C, 14.7 psig, W/F= 0.3 h, and TOS=3 h)

Feed	*ME	*ET	*PR	*BU
Conversion (%)	100	100	100	100
Oxygenate (mol_{carbon} %)	*2.66*	*3.37*	*3.82*	*2.63*
Acetaldehyde	0.0	0.0	0.0	0.1
Formaldehyde	0.0	0.0	0.0	0.0
Propanal	0.0	0.0	0.0	0.0
Acetone	2.66	0.0	0.49	2.63
Propenal	0.0	3.37	3.33	0.0
Methanol	0.0	0.0	0.0	0.0
Ethanol	0.0	0.0	1.0	0.0
n-Propanol	0.0	0.0	1.0	0.0
n-Butanol	0.0	0.0	0.0	0.0
Acetic	0.0	0.0	0.0	0.0
Propanoic	0.0	0.0	0.0	0.0
Heavy oxygenate	0.0	0.0	0.0	0.0
Hydrocarbon (mol_{carbon} %)	*97.34*	*96.63*	*96.19*	*97.37*
C1-C3 Paraffins	*4.35*	*8.91*	*20.47*	*19.15*
C4+ Paraffins	*29.08*	*6.90*	*8.58*	*6.63*
Ethylene	*3.21*	*7.56*	*2.84*	*2.50*
Propylene	*3.99*	*11.24*	*4.14*	*3.58*
Butene	*0.83*	*2.86*	*0.91*	*1.31*
Benzene	*5.58*	*8.66*	*9.37*	*9.18*
Toluene	*26.46*	*27.67*	*31.05*	*30.00*
EB	*0.44*	*1.92*	*0.60*	*3.61*
p-Xylene	*4.57*	*4.09*	*3.67*	*3.98*
m-Xylene	*10.32*	*9.28*	*7.53*	*9.21*
o-Xylene	*4.93*	*4.18*	*3.97*	*4.17*
C9Aromatics	*0.00*	*2.32*	*1.15*	*3.00*
C10Aromatics	*2.42*	*0.68*	*1.21*	*1.06*
C11Aromatics	*0.62*	*0.17*	*0.35*	*0.00*
C12Aromatics	*0.55*	*0.07*	*0.22*	*0.00*
C13Aromatics	*0.00*	*0.12*	*0.13*	*0.00*

*ME = methanol, ET = ethanol, PR = *n*-propanol and BU = *n*-butanol

Figure 4.13 shows the temperature-programmed oxidation (TPO) profiles of spent HZSM-5 with different biomass-derived alcohols, which carries out at 450 °C, atmospheric pressure and N_2/feed molar ratio of 1.4 after 9 h TOS. Table 4.7 summarizes the amount of coke formed over the different biomass-derived alcohols. It was clearly seen that amount of coke deposited on catalyst and the strength of coke (oxidation temperature) were decreased in following order of: *n*-butanol. > *n*-propanol> ethanol > methanol. The result indicated that amount of coke deposition was directly related to aromatics selectivity and the natures of coke are similar all of feedstocks.

Table 4.7 Amount of coke formed on the HZSM-5 with different biomass-derived alcohols

Feed (HZSM-5)	Coke (wt.%)
Methanol	5.53
Ethanol	6.45
n-Propanol	8.84
n-Butanol	10.43

4.3.2 Effect of Concentration of Alkali Treatment

The influences of NaOH concentration used in the alkali treatment on the properties of HZSM-5 zeolites have been studied in a range of 0–1.0 M at 75 °C treatment time for 2 h. The aim of alkali-treatment is to improve the diffusion ability of zeolites and enhanced aromatics selectivity. Figure 4.14 shows the alkali-treated HZSM-5 exhibited relatively higher aromatics selectivity except 1 ATHZ.

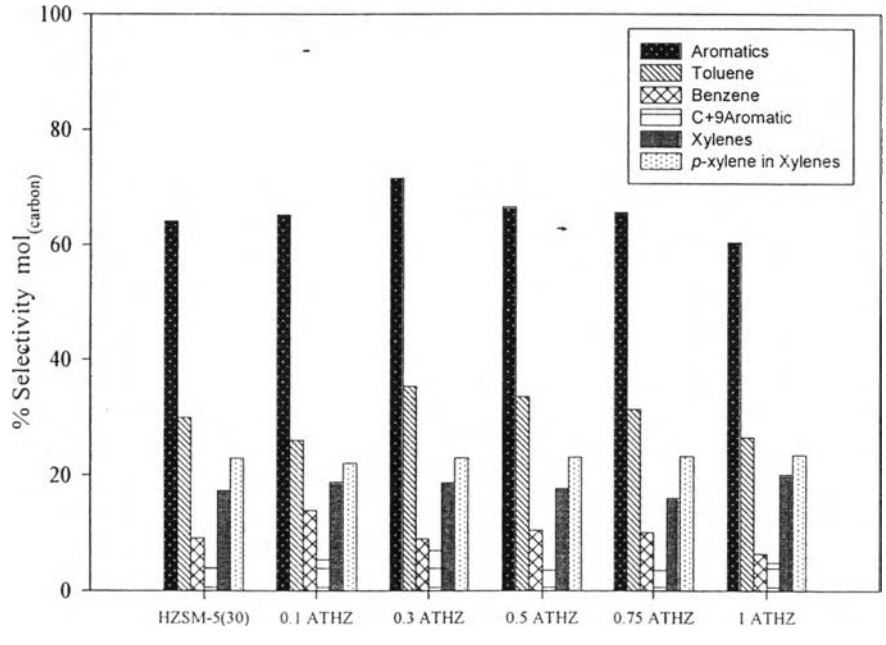

Figure 4.14 Effect of concentration NaOH solution on aromatic products selectivity and *p*-xylene selectivity in xylenes (Reaction conditions: 450 °C, 14.7 psig, W/F= 0.3 h, and TOS = 3 h).

The results indicated that the product distributions after 3 h of time on stream are shown in Table 4.8. The aromatics selectivity was decreased on the following order of 0.3 ATHZ > 0.5 ATHZ > 0.1 ATHZ > 0.75 ATHZ > HZSM-5, and 1 ATHZ. The damage to micropores was not severe. The acid property was changed after treated the HZSM-5 zeolite with 0.1-0.3 M NaOH which may be beneficial to the selectivity to aromatics. However, the alkali treatment with 1 M NaOH caused a severe damage to micropores which may be unfavorable to aromatization. This is probably due to the HZSM-5 structure was destroyed, leading to the lower aromatization selectivity (Ni *et al.*, 2011).

Over the properly alkali-treated HZSM-5 zeolites, the reaction activity was enhanced. Both the micropores and mesopores of the catalyst can be improved the aromatics selectivity; the former ensures the shape-selectivity, while the latter maintains the shorter path length thus reducing the channel blockage. The coke produced, soft and hard coke in the reaction procedure tends to deposit in the micropores and mesopores of the zeolites (Li *et al.*, 2008).

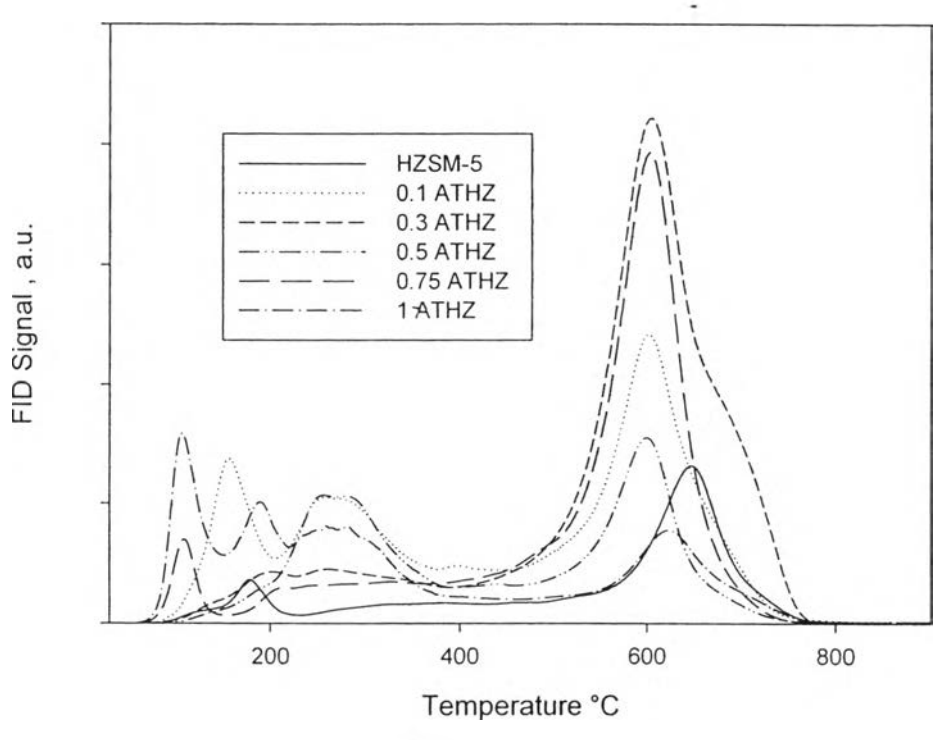

Figure 4.15 TPO profiles of spent HZSM-5 various concentration NaOH solution (Reaction conditions: 450 °C, 14.7 psig, W/F= 0.3 h, and TOS = 3 h).

Table 4.8 The product yields and conversion of *n*-butanol obtained over the alkali treated on HZSM-5 with various concentrations (Reaction conditions: 450 °C, 14.7 psig, W/F= 0.3 h, and TOS=3 h)

Concentration (Molar)	0.1	0.3	0.5	0.75	1
Conversion (%)	100	100	100	100	100
Oxygenate (mol_{carbon} %)	*- 0.92*	*0.0*	*0.0*	*0.31*	*0.31*
Acetaldehyde	0.0	0.0	0.0	0.1	0.1
Formaldehyde	0.0	0.0	0.0	0.0	0.0
Propanal	0.0	0.0	0.0	0.0	0.43
Acetone	0.0	0.0	0.0	0.0	0.19
Propenal	0.92	0.0	0.0	0.31	0.20
Methanol	0.0	0.0	0.0	0.0	0.0
Ethanol	0.0	0.0	1.0	0.0	0.0
n-Propanol	0.0	0.0	1.0	0.0	0.0
n-Butanol	0.0	0.0	0.0	0.0	0.0
Acetic	0.0	0.0	0.0	0.0	0.0
Propanoic	0.0	0.0	0.0	0.0	0.0
Heavy oxygenate	0.0	0.0	0.0	0.0	0.0
Hydrocarbon (mol_{carbon} %)	*99.08*	*100.00*	*100.00*	*99.69*	*99.18*
C1-C3 Paraffins	*15.68*	*8.92*	*18.61*	*16.93*	*19.61*
C4+ Paraffins	*8.77*	*7.03*	*6.90*	*7.68*	*11.45*
Ethylene	*3.33*	*3.88*	*2.66*	*3.13*	*2.34*
Propylene	*4.84*	*6.74*	*3.89*	*4.63*	*4.25*
Butene	*1.20*	*1.81*	*1.32*	*1.69*	*1.17*
Benzene	*13.97*	*9.04*	*10.52*	*10.11*	*6.46*
Toluene	*26.01*	*35.34*	*33.59*	*31.35*	*26.52*
EB	*1.03*	*1.48*	*1.14*	*4.51*	*2.38*
p-Xylene	*4.15*	*4.31*	*4.10*	*3.73*	*4.72*
m-Xylene	*10.04*	*9.97*	*9.34*	*8.45*	*10.62*
o-Xylene	*4.61*	*4.46*	*4.29*	*3.88*	*4.76*
C9Aromatics	*1.79*	*0.67*	*1.61*	*2.06*	*4.12*
C10Aromatics	*2.46*	*2.52*	*1.71*	*1.45*	*0.77*
C11Aromatics	*0.24*	*0.26*	*0.11*	*0.09*	*0.00*
C12Aromatics	*0.58*	*2.32*	*0.20*	*0.00*	*0.00*
C13Aromatics	*0.37*	*1.24*	*0.00*	*0.00*	*0.00*

The TPO profiles of carbon deposited on the parent HZSM-5 and alkali treated HZSM-5 are shown in Figure 4.15. It was clearly seen that amount of coke deposited on catalyst was decreased in following order of: 0.3 ATHZ > 0.5ATHZ > 0.1ATHZ > HZSM-5 > 0.75 ATHZ > 1 ATHZ. The result indicated that amount of coke deposition was directly related to aromatics selectivity and the natures of coke consist of soft coke and hard coke for all catalysts modification.

Table 4.9 Amount of coke formed on the alkali treated HZSM-5 with different concentration

Catalysts (*n*-Butanol)	Coke (wt.%)
HZSM-5	10.43
0.1ATHZ	9.89
0.3ATHZ	19.97
0.5ATHZ	13.02
0.75ATHZ	10.60
1 ATHZ	8.40

4.3.3 Effect of CLD Cycle Number on HZSM-5 Catalysts

The *p*-xylene selectivity was enhanced due to the deposition of inert silica layer on the external surface of HZSM-5 zeolite. The effects cycle number was studied by chemical liquid deposition (CLD) method. Amount of TEOS (1.0) mL per gram catalyst denoted as 20CLD, 0.3AT20CLD and CLD cycle number (2 cycles of 0.5 ml of TEOS per gram catalyst denoted as 2Cy20CLD) were dissolved in 20 vol.% of TEOS in cyclohexane. The *n*-butanol conversion and aromatic yield are shown in Figure 4.16. It can be seen that the *p*-xylene selectivity in xylenes was enhanced with silylation method. The increase in *p*-xylene selectivity in xylenes can be attributed to the chemical liquid deposition (CLD) resulted in deactivation of external acid sites and also fine control of zeolite pore opening, which affects the diffusion of the bulkier ortho and meta xylene isomers out of the channels. Hence of the xylenes formed inside the channels of the zeolite, the para isomer, being the smallest in size, is the easiest to exit. Both meta and ortho were to get converted to para by isomerization before they diffuse out from the pores (Yajnavalkya et. al., 1995). For the CLD cycle number, the two-cycle of TEOS deposition (2x0.5CLD20) showed higher *p*-xylene selectivity in xylenes than one cycle of TEOS deposition (20CLD) at the same amount of TEOS per mass of catalyst. It was implied that, multi-cycle deposition could increase the amount of silica deposited on HZSM-5 zeolite external surface.

Although, the conversion of *n*-butanol was achieved at 100% in all silylated HZSM-5 catalysts as shown in Figure 4.16, but the yield of aromatics was decreased with increasing the *p*-xylene selectivity in xylenes. It could explain that the deposition of inert silica layer resulted in deactivation of external acid sites and also decreasing both surface areas of zeolite and Brønsted acid sites as mentioned in Table 4.3 and 4.5. It was well known that the decrease in surface area resulting in decreasing of the active surface. This could be became it was suggested that the transformation of olefin into aromatics is catalyzed only by strong acid sites over the ZSM-5 (Yueqin *et. al.* 2011).

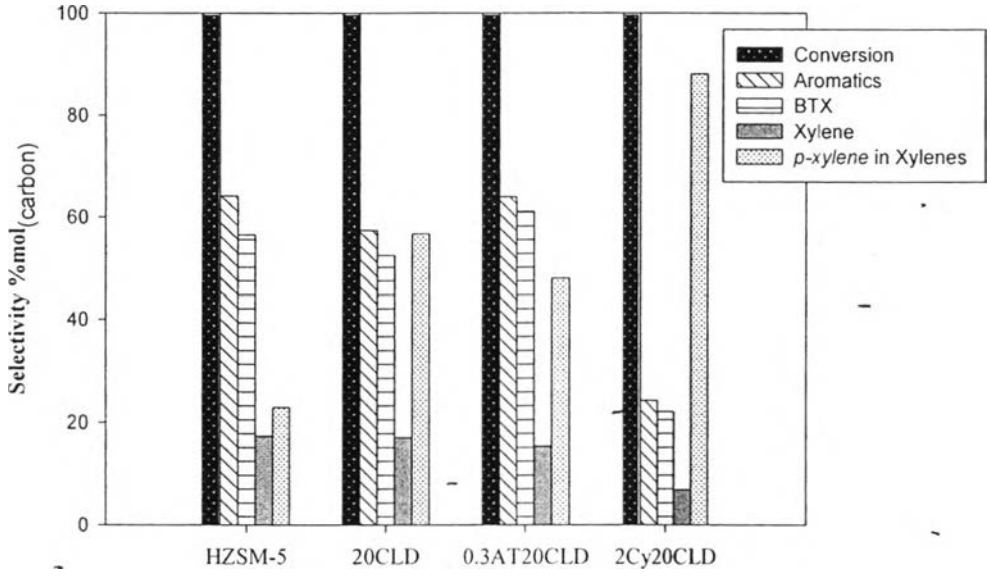

Figure 4.16 Effect of TEOS amount and cycle number on aromatic products selectivity and *p*-xylene selectivity in xylenes (Reaction conditions: 450 °C, 14.7 psig, W/F= 0.3 h, and TOS = 3 h).

The deposited silica on HZSM-5 was analyzed by XRF. Table 4.10 shows that the Si/Al ratio increased with increasing TEOS loading. The decrease in aromatics yields and increase in *p*-xylene selectivity in xylenes were proportional to the amount of Si and SiO_2/Al_2O_3 molar ratio

Table 4.10 The amount of deposited silica on the parent and silylated HZSM-5(30)

Catalysts	Aromatics yield (mol_{carbon}%)	*p*-Xylene selectivity in xylenes (%)	Si/Al molar ratio
HZSM-5(30)	64.2	22.9	31.6
20CLD	57.4	56.7	32.8
0.3AT20CLD	64.0	49.0	35.1
2Cy20CLD	24.3	88.1	48.9

Table 4.11 Amount of coke formed on the parent and silylated HZSM-5(30) zeolites after 9 h TOS

Catalysts (*n*-butanol)	Coke (wt.%)
HZSM-5 (30)	10.43
20CLD	10.92
0.3AT20CLD	13.61
2Cy20CLD	6.73

The TPO profiles of carbon deposited on the parent HZSM-5 and silylated HZSM-5(30) are shown in Figure 4.17. It was clearly seen that the amount of coke deposited on catalyst was decreased in following order of: HZSM-5(30) > 20CLD > 0.3AT20CLD > 2Cy20CLD. The result indicated that amount of coke deposition was directly related to the aromatics yield.

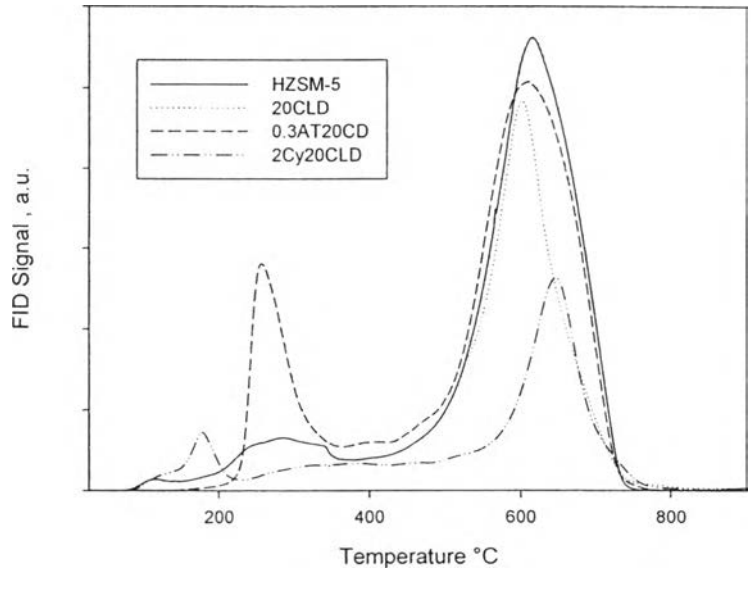

Figure 4.17 TPO profiles of spent a) parent HZSM-5(30), b) 20CLD, c) 0.3AT20CLD and d) 2Cy20CLD (Reaction conditions: 450 °C, 14.7 psig, W/F= 1.0 h, and after 9 h TOS).

Table 4.12 The product yield and conversion of glycerol obtained over the parent and silylated HZSM-5(30) (Reaction conditions: 450 °C, 14.7 psig, W/F= 0.3 h, and TOS=3 h)

Catalysts	HZSM-5(30)	20CLD	0.3AT20CLD	2Cy20CLD
Conversion (%)	100	100	100	100
Oxygenate (mol_{carbon} %)	*2.63*	*0.52*	*0.75*	*0.0*
Acetaldehyde	0.1	0.30	0.75	0.0
Formaldehyde	0.0	0.0	0.0	0.0
Propanal	0.0	0.14	0.0	0.0
Acetone	2.63	0.0	0.0	0.0
Propenal	0.0	0.0	0.0	0.0
Methanol	0.0	0.09	0.0	0.0
Ethanol	0.0	0.0	0.0	0.0
Alkyl alcohol	0.0	0.0	0.0	0.0
Acetol	0.0	0.0	0.0	0.0
Acetic	0.0	0.0	0.0	0.0
Propanoic	0.0	0.0	0.0	0.0
Heavy oxygenate	0.0	0.0	0.0	0.0
Hydrocarbon (mol_{carbon} %)	*97.34*	99.48	*99.25*	*100.00*
C1-C3 Paraffins	*4.35*	10.40	13.42	11.32
C4+ Paraffins	*29.08*	19.51	14.21	29.63
Ethylene	*3.21*	2.14	1.90	0.77
Propylene	*3.99*	5.69	3.70	18.39
Butene	*0.83*	4.32	2.00	15.65
Benzene	*5.58*	3.29	12.78	0.32
Toluene	*26.46*	32.12	32.98	14.93
EB	*0.44*	2.58	1.72	0.66
p-Xylene	*4.57*	9.66	7.39	6.02
m-Xylene	*10.32*	6.11	6.45	0.00
o-Xylene	*4.93*	1.28	1.56	0.81
C9Aromatics	*0.00*	2.34	0.67	0.00
C10Aromatics	*2.42*	0.00	0.00	0.00
C11Aromatics	*0.62*	0.00	0.00	0.00
C12Aromatics	*0.55*	0.04	0.30	0.97
C13Aromatics	*0.00*	0.02	0.16	0.53

4.3.4 Proposed Reaction Pathway for Aromatization of Biomass-derived Alcohol (Ethanol and *n*-Butanol)

Transformation of biomass-derived alcohols over HZSM-5 with SiO_2/Al_2O_3 ratio 30 as a function of space time (W/F) at 400 °C and atmospheric pressure under nitrogen flow. For ethanol and *n*-butanol, it can be observed that, at low contract time, the main reaction is dehydration to ethylene and butene, which are the primary product. These hydrocarbons are formed at moderate temperatures (between 250 and 400 °C) by reactions of oligomerization, alkylation, hydrogen transfer, cyclization, and isomerization, however at above 400 °C, cracking also occurs. The higher the molecular weight, the higher probability of the cracking reaction, as following orders of olefins > paraffins > aromatics (Gayubo *et al.*, 2004).

The ethanol to hydrocarbon reaction over a HZSM-5 catalyst consists of two main steps; dehydration to ethylene and the further conversion to a higher hydrocarbon fraction. Figure 4.18 shows the dehydration of ethanol taken place by two competitive paths: intramolecular dehydration to ethylene directly and second intermolecular dehydration to diethylether followed by dehydration of diethylether to ethylene respectively (Stefaan Stevens, 2010).

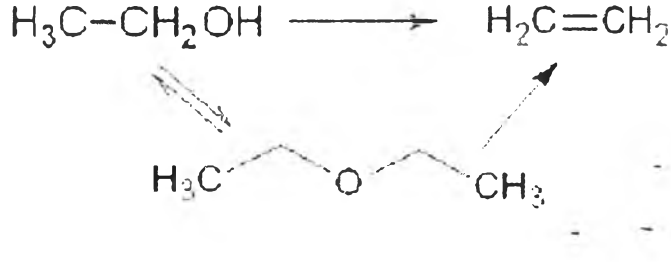

Figure 4.18 Dehydration of ethanol (Stefaan Stevens, 2010).

Taking into account the proposed reaction pathways, the principal scheme of ethanol to hydrocarbon conversion was proposed in Figure 4.20. The product mixture consisted of ethylene, propylene, butane, diethylether, paraffin (C4+), olefin (C5+), and aromatics (mainly C6-C8) (Inaba *et al.*, 2006).

Increasing W/F leading to the dehydration of ethylene and C4 olefin, that could undergo further reactions such as oligomerization, aromatization, and hydrogen transfer or cracking, which gave higher hydrocarbons (olefins, paraffins and BTX). Some hydrocarbons may be transformed to deposited carbon by excess reaction (Inaba *et al.*, 2006).

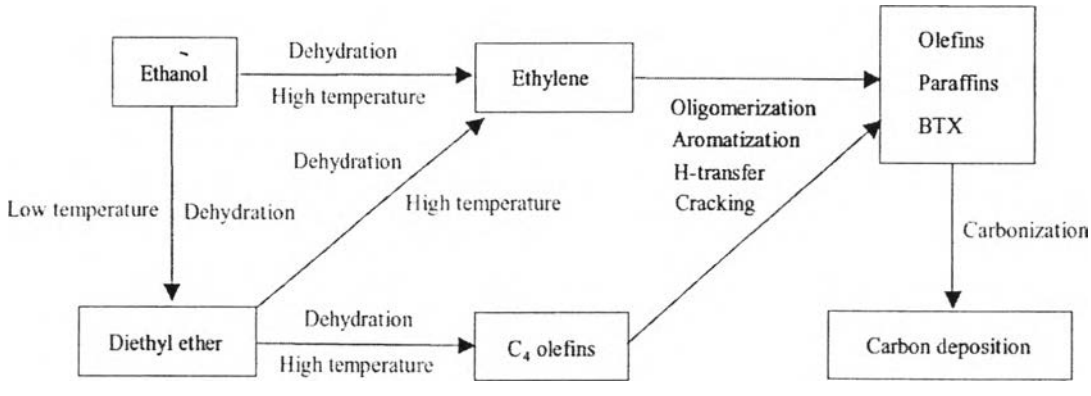

Figure 4.19 Supposed reaction pathway of ethanol (Inaba *et al.*, 2006).

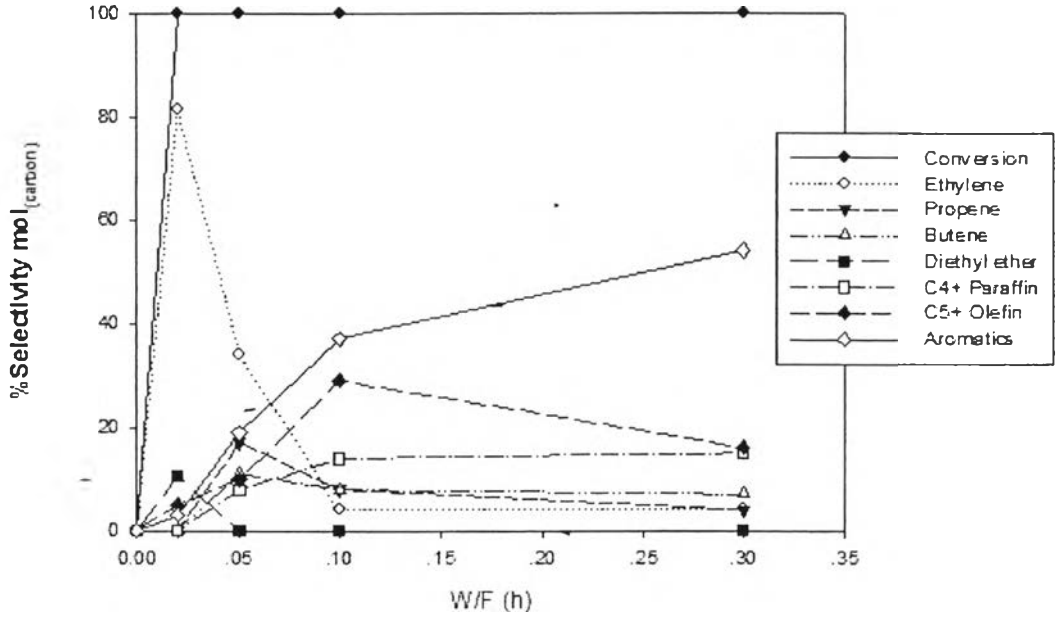

Figure 4.20 Product yield of ethanol conversion over HZSM-5 with SiO_2/Al_2O_3 ratio of 30 as a function of space time (W/F) at 400 °C, 14.7 psig, and TOS = 3 h.

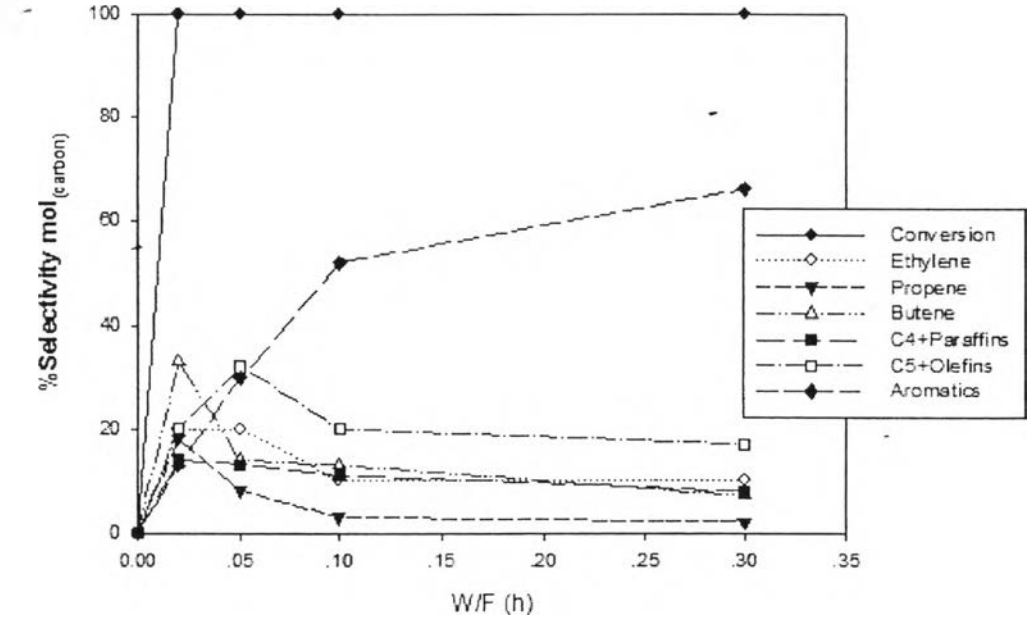

Figure 4.21 Product yield of *n*-butanol conversion over HZSM-5 with $SiO_2/Al2O_3$ ratio of 30 as a function of space time (W/F) at 400 °C, 14.7 psig, and TOS = 3 h.

Figure 4.22 shows the product distribution of *n*-butanol by varying space time. It can be seen that *n*-butanol was completely convert 100%, the maximum observed in the gaseous (ethylene propylene and butene) and nonaromatic (C4+ paraffin and C5+olefin). Liquid yields evidences that these products were intermediate in the reaction pathway. Aromatic hydrocarbons were increased at high space time. At the lowest W/F of 0.02 h the dehydration of *n*-butanol has a maximum net yield of butene of 33% at 400 °C, butene is the first product obtained in the dehydration of *n*-butanol. Olefins, butenes, and C5+ olefins are almost exclusively formed, even for this space time (Gayubo *et al.*, 2004).

Increasing W/F leading to the dehydration of *n*-butanol that could undergo butenes which can be transformed into higher olefins and C5+ of olefins, and these C5+ are an intermediate product for produce aromatics. The C4+ paraffins were obtained by alkylation, isomerization, and hydrogen-transfer reactions and the aromatics were obtained by cyclization, dehydrogenation, and aromatization reactions (Varvarin *et al.*, 2013).

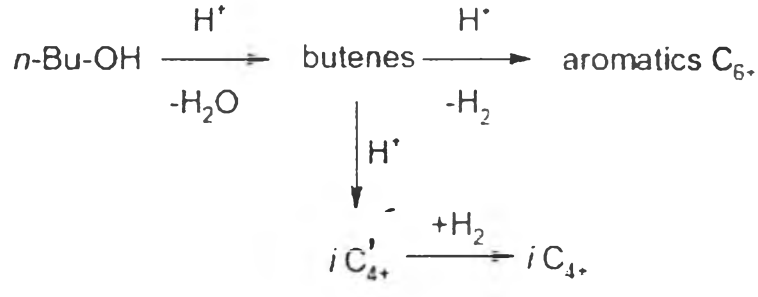

Figure 4.22 Supposed reaction pathway of *n*-butanol (Varvarin *et al.*, 2013).